1D nanoporous membrane boosts the ionic conductivity of electrolytes

Nino Modesto [a,b,c,d,1], Camille Pinchart [a,b,1], Mohammad Abdel Sater [a,b,e,f], Markus Appel [g], Peter Fouquet [g], Alessandro Tengattini [g,h], Margarita Russina [i], Veronika Grzimek [i], Gerrit Günther [i], Pierre-Henri Jouneau [e], Benoit Coasne [g,j], Didier Lairez [b,k], Patrick Judeinstein [b,f], Raphael Ramos [l], Didier Gigmes [c], Trang N.T. Phan [c], Quentin Berrod [a] (ID),*, Jean-Marc Zanotti [b,*]

a University Grenoble Alpes, CNRS, CEA, Grenoble INP, IRIG, SyMMES, Grenoble, 38000, France
b Universite Paris-Saclay, CEA, CNRS, Laboratoire Leon Brillouin, CEA Saclay, Saclay, France
c Universite Aix Marseille, CNRS, Institut de Chimie Radicalaire, Marseille, France
d Blue Solutions, Ergue Gaberic, 29500, France
e University Grenoble Alpes, CNRS, CEA, IRIG, MEM, Grenoble, 38000, France
f Universite Paris-Saclay, Laboratoire de Physique des Solides, Orsay, France
g Institut Laue Langevin, Grenoble, 38000, France
h University Grenoble Alpes, CNRS, Grenoble INP, 3SR, Grenoble, 38000, France
i Helmholtz-Zentrum Berlin, Berlin, Germany
j University Grenoble Alpes, CNRS, LIPhy, Grenoble, 38000, France
k Laboratoire des solides irradies, Ecole polytechnique, CEA, CNRS, IPP, Palaiseau, 91128, France
l University Grenoble Alpes, CEA, LITEN, Grenoble, 38000, France

ARTICLE INFO

ABSTRACT

Solid-state batteries have attracted significant interest as promising candidates for high energy density and safe battery technology. However, they commonly experience low ionic conductivity at ambient temperature, which limits their power density. This study addresses this issue by developing a porous separator with one-dimensional (1D) nanometric channels that confine non-flammable ionic liquid-based electrolytes (IL-Li). We achieve 1D macroscopic ionic transport by confining the electrolytes within Vertically Aligned Carbon NanoTubes (VA-CNT) composite membranes. Employing quasi-elastic neutron scattering techniques, we conduct a multiscale analysis of the diffusive motion of both bulk and confined electrolytes. By extracting diffusion coefficients spanning from the molecular to macroscopic scale, we gain insights into the transport properties of IL-Li. Our results show that nanometric confinement allows to lower the operational temperature of these electrolytes by up to 20 K compared to the non-confined electrolytes. At ambient temperature, we show a tenfold increase in conductivity under 1D CNT confinement. Molecular Dynamics simulations shed light on the underlying physics, showing a unique intermolecular organization of the IL-Li under confinement. Specifically, the molecules form a core–shell structure, resulting in the creation of quasi-1D transport channels. This study presents promising avenues for exploring the use of 1D materials in energy storage applications.

1. Introduction

Batteries designed for electric vehicles should be able to provide both high specific energy and power. Supercapacitors deliver relatively high specific power densities (10^4 W/kg) but at the expense of the specific energy they can store (10 Wh/kg). At the opposite, in comparison to other electrochemical storage systems, lithium batteries show very high specific energy (300 Wh/kg) but with low specific power (100 W/kg) so that this energy can be delivered only slowly resulting in an instant power below the expectations [1]. Accordingly, a gap appears in the Ragone Power/Energy plot because no system fulfills both power and energy capabilities demanded by the transportation systems needs.

All-solid-state lithium batteries have attracted growing attention in the last decade [2]. Rather than liquid or gelified electrolytes, these devices take advantage of the properties of solid ones. They offer

---

a number of benefits over their liquid-based analogs in terms of (i) improved safety [3], (ii) extended lifetime [4], (iii) better performances at extreme temperatures [5], and (iv) lower weight [6]. However they usually suffer from poor ionic conductivity leading to low power density.

Dong et al. have recently reported a significant ionic conductivity enhancement by confining Ionic Liquids (ILs) into two-dimensional (2D) materials-based membranes [7]. They show that under such 2D nanometric confinement the ILs diffusion behavior is remarkably accelerated by a factor 1.5 to 5. Here, we use VA-CNT (Vertically Aligned Carbon Nanotube, where vertically refers only to CNT growth on its substrate) array to extend this reduction of dimensionality to its physical limit and design a one dimension (1D) nanoporous all-solid-state lithium battery separator. We consider two imidazolium based ILs: 1-butyl-3-methylimidazolium bis(trifluoro methanesulfonyl) imide (BmimTFSI) and 1-methyl-3-octylimidazolium bis(trifluoro methanesulfonyl) imide (OmimTFSI), both charged with 1 M of lithium bis(trifluoro methanesulfonyl) imide (LiTFSI), hereafter referred to as Bmim-Li and Omim-Li, respectively. In bulk, due to competition between the electrostatic and van der Walls interactions of their aliphatic side chains, 4 and 8 carbons respectively, they spontaneously organize in transient nanometric domains. The phenomenon is evidenced in diffraction by a so called pre-peak in the 0.1–0.3 Å^{-1} region [8]. It is much more clearly defined for neat Omim than Bmim and is increased upon lithium addition [9]. This nanometric structuration forms transient energy barriers that prevent the free diffusion of charges with a strong detrimental consequence on the anionic diffusivity [10,11]. As they significantly differ by their physical properties, we address in the present paper both Bmim-Li and Omim-Li based systems.

Addressing nanometric confinement of a molecular fluid within a porous material comes to consider both the molecule and the pore characteristic sizes, a and Φ_{Pore} respectively. Confinement is a notorious way to induce strong depression of the melting point (Gibbs–Thomson effect). Below the melting point, for a crystalline material when ($\Phi_{Pore} \gg a$) the relevant parameter becomes the typical size of a crystallite. Above the melting point, if the confined liquid can self-organize, the relevant dimension is the one of the transient or stable supra-aggregates the molecules can form. If their characteristic size is larger than the pore one, new physical properties can be obtained compared to the bulk fluid [12–14]. In this work, the frustration of the natural self-organization of Bmim-Li and Omim-Li under CNT confinement will serve as an additional control parameter to further enhance the 1D transport properties.

A main challenge in confined systems is to firmly bridge the local structure and short time dynamics to the macroscopic properties. In an electrolyte, the transport properties, in particular the translational diffusion coefficient and the conductivity of the ionic species, are related by the Nernst-Einstein relation [15–17]. In this paper, we focus on those two quantities, obtained experimentally by using Quasi-Elastic Neutron Scattering (QENS), Pulsed Field Gradient NMR, and conductivity measurements. First, we describe the preparation of the 1D CNT nanoporous membrane and how IL based electrolytes (designated as IL-Li) fill the CNT pores. Then, QENS show a downshift of the melting temperature of the IL-Li and an increase by a factor of 2 of the IL dynamics. The ionic conductivity of Omim-Li is found to be enhanced by an order of magnitude under CNT confinement. This two results improves considerably the performances of IL-Li. Finally, Molecular Dynamics (MD) is used to support our interpretation of the experimental results. While our previous study focused on the translational diffusion coefficients of neat IL at room temperature [18], this work directly addresses the ionic conductivity of electrolyte relevant for battery applications: IL charged with lithium salt under CNT confinement. Moreover, based on the MD simulations we speculate on the physical reasons behind the enhanced conductivity and provide insights into the confining geometry required to achieve such properties.

2. Experimental section

2.1. CNT membrane synthesis

VA-CNT arrays were synthesized by chemical vapor deposition (CVD) via the two-step catalyst-supported technique. A 1-nm-thick iron catalyst thin film is first deposited by e-beam evaporation on an alumina-covered silicon wafer (10 nm thick alumina by atomic layer deposition). For the growth of high areal density VA-CNT array on this substrate, an original implementation of hot-filament-assisted CVD in which the filaments are made out of carbon was used with acetylene carbon precursor. As reported elsewhere [19], this specific process allows the growth of high density arrays of small diameter multiwall CNTs which are not obstructed by internal graphenic walls and thus well suited for 1D macroscopic ionic transport [20]. The fabrication of nanoporous composite membrane starting from the supported VA-CNT array is described in the main text.

2.2. Electrolytes

BmimTFSI ($\geq$ 99.5%) and OmimTFSI ($\geq$ 99%) were purchased from Iolitec, stored under Ar and used as received in a glovebox. LiTFSI salts ($\geq$ 99.95%) were purchased from Sigma Aldrich (Merck) and dried over night in a buchi glass oven under vacuum, before entering the glovebox under argon atmosphere. The O_2 and H_2O content was less than 10 ppm and 1 ppm, respectively. The electrolytes were prepared as followed. In a sealed vial, on a stirring hot plate, 2.87 g of LiTFSI were solubilized in 10 mL of ionic liquid to reach a molar concentration of 1M. After solubilization, a tri-neck round bottom flask linked to a vacuum pump was filled with the electrolyte. The CNT membranes were then immersed in the electrolyte and the flask was put under vacuum for 1 h. The excess electrolyte is then removed by gently patting it dry. This methodology is used for QENS, NMR, and conductivity measurements.

2.3. Raman scattering

Raman analysis were conducted with a Renishaw In Via confocal micro-Raman system in backscattering configuration with 0.5 NA (numerical aperture) objective. Laser excitation at 785 nm was used with low power on the sample to prevent sample heating or degradation ($<$ 0.25 mW/μm^2). The spatial resolution of $\sim$ 2 μm allows localized interrogation of CNT-rich area of the membrane cross sections.

2.4. NMR

NMR experiments were performed at 9.4T, with a Tecmag spectometer equipped with a DOTY PFG probe. Membranes materials were cut in small square shape elements (around 3 mm $\times$ 3 mm) which are stacked inside a standard 5 mm NMR tube. Measurements have been performed with CNT tubes oriented parallel and orthogonal to the magnetic field, and very few differences are measured, then only parallel spectra are presented and discussed.

2.5. Neutron imaging

Neutron Imaging experiments were performed on NeXT at ILL. Strong contrast enhancement can be achieved by selectively replacing hydrogen by deuterium within the target structure. We have prepared a VA-CNT membrane with deuterated polystyrene (PS-D), while the IL-Li were hydrogenated. Two samples have been prepared at the same time under the same conditions (duration, temperature, drying time): the deuterated VA-CNT membrane with pores open on both side and a PS-D "only" membrane, used as a reference. The samples are measured successively in the same measuring aluminum cell. For each of them, the neutron intensity is measured over time, after an IL-Li drop is deposited on the top of the membrane. Home made experimental cell
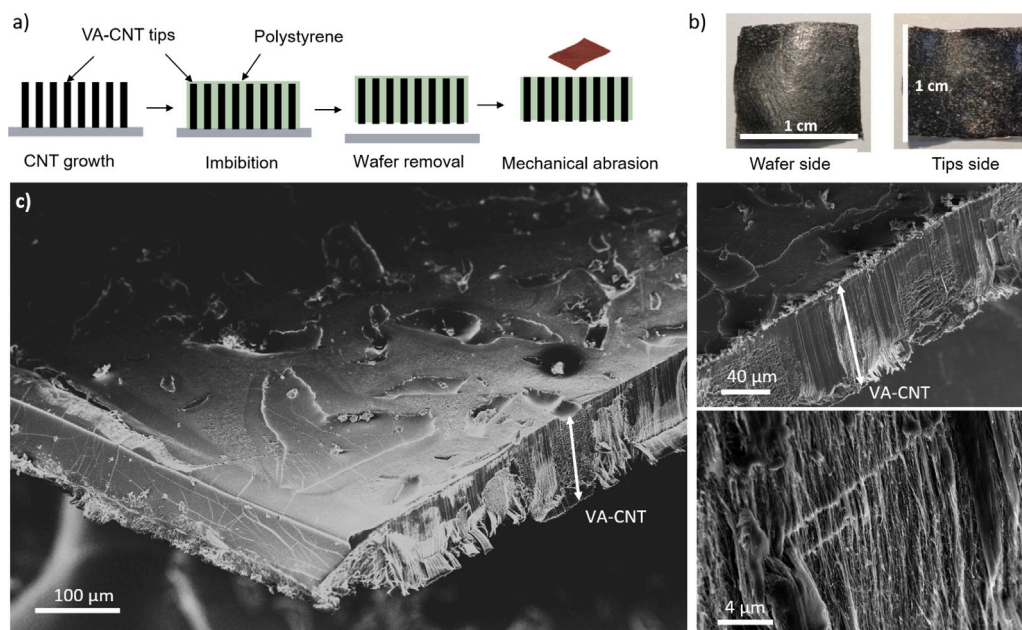
Fig. 1. (a) Schematic process of a porous composite membrane manufacturing. The porous moiety is the CNT cores. (b) Pictures of wafer and tip side of a real membrane. (c) SEM image of the membrane showing the VA-CNT embedded in the polymer matrix.

was used to hold the membrane parallel to the beam (see Figure S1). The IL-Li drop is added on one side while pumping (pressure 100 mbar) on the other side. Tightness is guaranteed by Teflon o-ring on each side of the membrane. Neutron imaging pictures have been corrected by Flat data (Flat Field Correction: measure without sample) and Dark data (Dark Field Correction: measure with no neutrons) as follow: $I = (I_{raw} - I_{dark})/(I_{flat} - I_{dark})$.

2.6. QENS

QENS experiment were performed on the following spectrometers: SHARP at ILL (time-of-flight spectrometer, resolution 70 μeV) [21,22], IN16B at ILL (backscattering spectrometer, resolution 0.7 μeV) [23,24], WASP at ILL (neutron spin echo spectrometer) [25], and NEAT at HZB (ToF, 100 μeV and 30 μeV resolutions) [26,27]. Bulk ionic liquids were sealed with indium joints in annular aluminum containers, while CNT membrane were sealed in specifically designed aluminum flat container to probe the dynamics alongside or perpendicular to the CNT (Fig. 5) [18]. ToF and BS acquired data were converted to $S(Q, \omega)$ spectra using the Mantid software [28], and Igor for WASP [29]. The treated data are then fitted with home developed QENSH software. Resolution function were measured at 2 K on WASP where we used TiZr (flat and cylindrical according to the sample geometry).

2.7. Molecular dynamics simulations

The MD simulations were carried out with a force field from the literature and a rigid carbon nanotube, interactions between the nanotube and the ionic liquid being described by repulsion-dispersion interactions in using a Lennard-Jones potential, in which the cross-parameters σ_{kj} and ϵ_{kj} between atom types k and j are obtained from the Lorentz–Berthelot mixing rules of like-atom pairs (Lennard Jones parameters for C: $\epsilon = 0.055642$ kcal mol^{-1}, $\sigma = 3.40$ Å) [30,31]. The simulations were carried out at 500 K in order to obtain an equilibrium regime and Fickian dynamics for reasonable trajectory durations. The trajectories were calculated for durations of 25 to 50 ns, with a step of 1 fs. Details are similar to those in the literature [9,32,33].

3. Results and discussion

3.1. Membrane preparation and characterization

In this work, we use a nanoporous composite polymer membrane to design a system offering 1D diffusion pathways for an electrolyte. Its synthesis and fabrication process has been described elsewhere [18]. It is summarized in Fig. 1. The key and basic component of this system is a VA-CNT array obtained by CVD (Chemical Vapor Deposition) onto a silicon wafer [20]. The intertube void space is soaked by a polymer solution composed of toluene and high molecular mass (350 kg mol^{-1}) polystyrene (PS) and then slowly (24–48 h) dried under vacuum. After complete drying, the membrane is detached out of its growth silicon support. At this stage, while all the CNT are open on the wafer side, the CNT tips are closed and covered by a polystyrene excess. In order to open the CNT and remove the PS excess, we carry out mechanical abrasion of the tip side of the membrane. At the end of the process we typically achieve 1 cm^2 membrane with a thickness of 100 μm.

3.2. Localization of the electrolyte within the CNT pores

Falk et al. have shown that in the case of CNT confined water, the friction coefficient driving the long range transport properties exhibits a strong curvature dependence: it decays with CNT radius for water inside nanotubes, but increases for water outside the nanotubes [14]. As our goal is to enhance the transport properties of the electrolyte, we have therefore paid special attention to make sure that the electrolytes are confined inside the CNT pores and not outside *i.e.* not in the polymer moiety of the membrane. This point has been investigated by the alliance of neutron imaging, Scanning Electron Microscope with Energy Dispersive X-ray Spectroscopy (SEM-EDX), Raman spectroscopy and Pulsed Field Gradient Nuclear Magnetic Resonance (PFG-NMR).

3.2.1. Nuclear magnetic resonance

In order to probe only the signal of the IL-Li protons, the NMR measurements have been conducted on membranes made of deuterated PS. With respect to the bulk, confinement leads to a major modifications of the NMR spectra: a strong increase of the linewidth. This is a general trend observed for molecular liquids under confinement [34]. A modification of the chemical shift (Fig. 2) is also noticeable in particular for
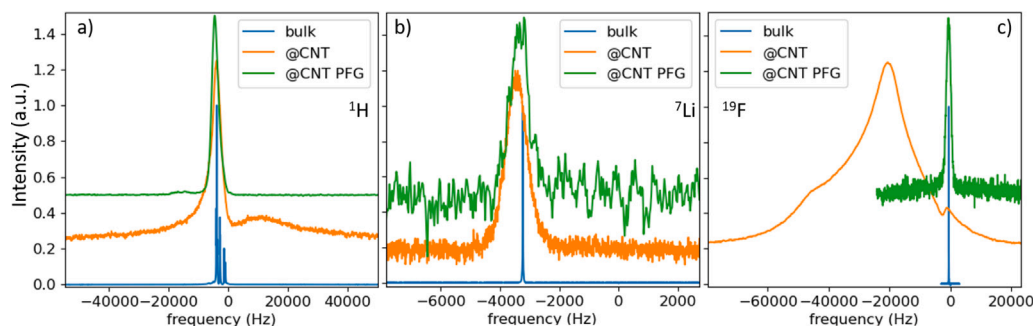
Fig. 2. ^1H (a), ^7Li (b) and ^{19}F (c) Omim-Li NMR spectrum at 300 K. The blue curve corresponds to the bulk Omim-Li, the confined signal is shown in orange. In the case of ^{19}F, the very broad signal corresponds to a component of the probe (Teflon). The confined signal filtered by the field gradient measurement is shown in green.

^1H and ^{19}F. Both effects are related to the intimate proximity of two medium (ionic liquid electrolytes and CNT nanotubes) with different magnetic susceptibilities, inducing an inhomogeneous magnetic field as well as strong magnetic gradient at interfaces. Moreover, ions at interface may experience anisotropic interactions, resulting in modified dipolar interactions and an increase in linewidth.

In the "filtered by field gradient measurement", the NMR spectrum is recorded after a specific diffusion coefficient measurement sequence and therefore modulated by the relaxation times T_1 and/or T_2 of the considered nuclei. The filtered signal is much weaker than the standard one. This difference corresponds to all the nuclei which relax quickly because of a lower mobility. While these NMR experiments show a clear signature of confinement, due to very short T_2 relaxation processes, reliable diffusion coefficient measurements of the three nuclei under investigation can nevertheless not be achieved. The shortening of the relaxation time compared to the neat IL under confinement is due to the addition of a significant amount of LiTFSI salt.

3.2.2. Neutron imaging

Neutron imaging (for a review in the field of batteries see [35]) is a non-destructive imaging technique using a white neutron beam to produce images of a material structure with a resolution of the order of 10 μm (7 μm in our case). The sample is enlighten by a neutron beam. By interaction with the sample, incident neutrons can be scattered or absorbed. Both processes are strongly isotopic dependant. In the context of this work, we use the strong difference of (*i*) the cross section of absorption of hydrogen, deuterium and empty CNT: $\sigma_a(H) = 0.0$ barn while $\sigma_a(D) = 0.3$ barn, and (*ii*) of their incoherent scattering cross-sections: $\sigma_{inc}(H) = 82$ barn while $\sigma_{inc}(D) = 7.6$ barn. The absorbed and scattered neutrons from the air inside the empty CNT is negligible. A membrane, where the polystyrene moiety is fully deuterated, is horizontally tightly hold between two jaws and topped by a reservoir of 1 mL of bulk hydrogenated Omim-Li (Fig. 3 and S1). A vacuum system placed underneath the membrane generates a pressure of approximately 100 mbar on its underside. The time dependence of the intensity detected by the CCD camera is shown in Fig. 3c and S3: as a function of time the transmitted intensity decreases. The same experiment is reproduced using a deuterated polystyrene film used to make the very same CNT membrane *i.e.* this membrane contains no CNT. In this case, the intensity remains constant over time. For the CNT membrane, the intensity loss is therefore solely due to imbibition of the hydrogenated Omim-Li. At the end of the process, drops of IL-Li can be seen on the bottom side of the membrane (see also Figure S2 for snapshots at different acquisition time). This is a strong evidence that (i) the composite membrane polymer moiety is free of any IL-Li and that (ii) the IL-Li is only confined in the CNT interior.

3.2.3. SEM-EDX and Raman spectroscopy

Prior to observation, a membrane has been filled with Omim-Li (Fig. 4 a,b) by vacuum imbibing. Fig. 4b shows a typical SEM image of a 100 μm thick membrane used for the identification of the location of the IL-Li. Different type of surfaces can be clearly distinguished. The region of the membrane seen in perspective (orange line), has been obtained by a simple scalpel cut. This type of treatment induces a very high roughness so that the details of the structure are too blurred to be analyzed over the full height. The front view surface (green) has been obtained by cryo-ultra microtomy. The clear cut results with no apparent roughness and produces a high quality image perfectly adapted to a detailed morphological and elemental analysis.

Two different moieties can be observed: some made solely of PS and others composed of VA-CNT bundles embedded in PS. These two phases correspond to a destructuration induced by the capillary densification of the CNT network upon the PS solution pouring onto the neat VA-CNT arrays. This process can actually be detected by eye at the moment of the pouring.

While in the pure PS (C_8H_8) region, EDX detects only carbon atoms (Figure S4), it highlights the presence of heavy atom in the CNT rich moieties: O: Oxygen, Sulfur: S, Fluorine: F (also shown as a mapping in green and red colors in Fig. 4c and Fig. 4d, respectively).

Different areas of the membrane containing VA-CNT and PS, as detected by an optical microscope integrated into the Raman spectrometer have been analyzed. The Raman spectra of these different zones are illustrated in Fig. 4e. Polystyrene, LiTFSI and VA-CNT are detected in the same area. This confirms the coating of the bundles by PS and the associated presence of LiTFSI. It should be noted that no significant spectral modifications were observed between the reference spectra of these three components (Figure S5) and their corresponding contributions in the composite membrane (Fig. 4e). By integration of the characteristic peaks, a quantitative analysis of the different contributions is possible: Fig. 4f shows a strong correlation between the presence of VA-CNT and LiTFSI.

3.3. Transport properties by quasi-elastic neutron scattering

The NMR, neutron imaging, SEM-EDX and Raman scattering experiments shown in the previous section, independently lead to the same and key conclusion: Omim-Li is not confined within the PS moiety but only in the 4 nm diameter VA-CNT. The same conclusion is obtained for Bmim-Li (not shown). Note that the above mentioned techniques do not have spatial resolution to refute that a small fraction of IL-Li could diffuse on the outside wall of the CNT. Due to interaction with the polymer matrix and convex curvature of the CNT, this hypothesis seems unlikely and could not explain the enhanced conductivity [14].

The transport properties of the IL-Li under 1D confinement can therefore be addressed. The classical technique to probe such quantities is PFG-NMR. At 300 K, in bulk, the self-diffusion coefficient of Omim-Li cation, D_{SDiff}, is found to be $1.6 \pm 0.3 \times 10^{-7}$ cm^2/s. Unfortunately, in the confined case, we have faced a very short T_2 time, as commonly observed for confined liquids. As a consequence, it has not be possible to assess the translational self-diffusion coefficients of the confined species at the micron scale.
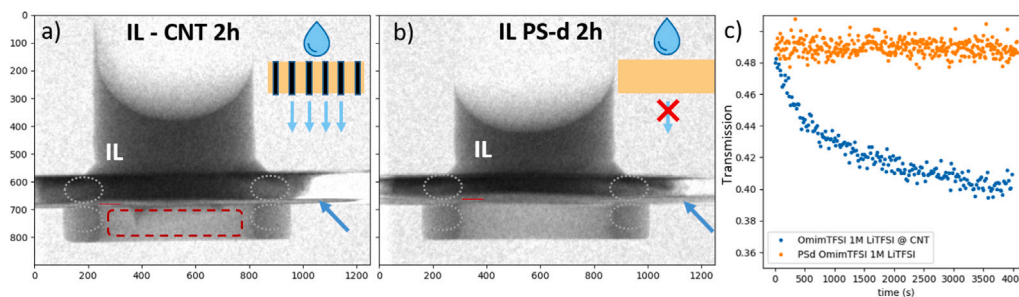
Fig. 3. Neutron radiography two hours after the deposit of an electrolyte drop onto (a) a CNT membrane and (b) a reference deuterated polystyrene (PS-d) film with no CNT. The opposite side of the electrolyte is under vacuum (100 mbar). Two o-rings (gray dashed line) prevent any leaking of the electrolyte by the side of the membrane. The electrolyte passing through the CNT membrane is highlighted in the red dashed rectangle. After two hours, no electrolyte is seen below the PS-d film (b). The blue arrow shows the CNT membrane in (a) and the PS-d film in (b). (c) Time dependence of the neutron transmission measured in the red area in a and b for the PS-d film (orange) and the CNT membrane (blue).
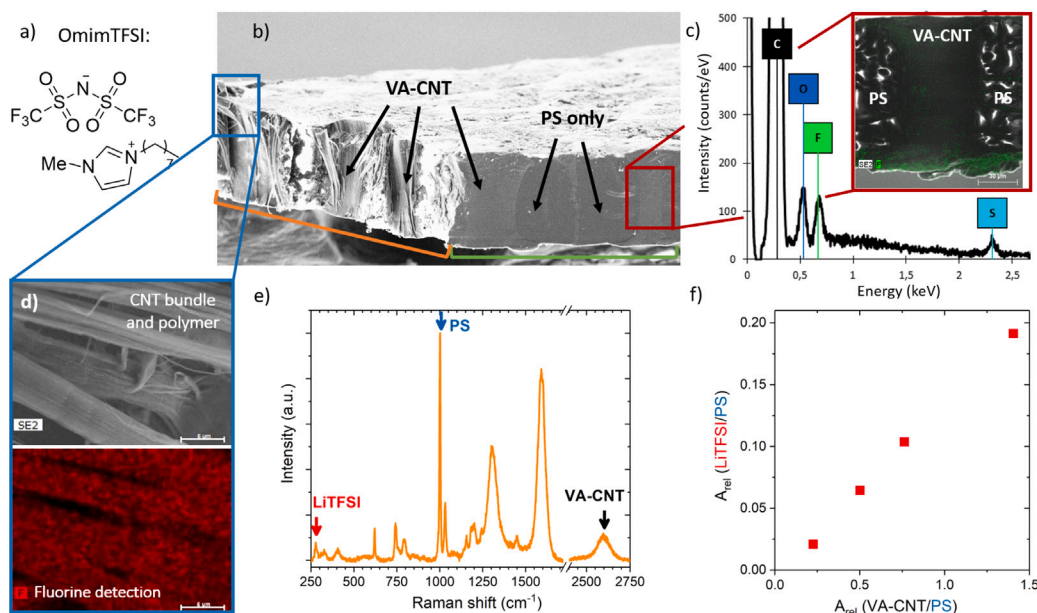

Fig. 4. (a) Structural formula of OmimTFSI. (b) SEM image of membrane imbibed by Omim-Li with in perspective a scalpel cut (orange line) and in front view (green line) a cut obtained by cryo-ultra microtomy. (c) Inset: a CNT rich area surrounded by two neat PS domains superimposed with EDX mapping (Fluorine, in green). Full EDX spectrum of the CNT rich phase showing C, O, F and S elements. (d) SEM and SEM/EDX mapping (F in red) of CNT bundles. (e) Raman spectrum from membrane cross-section. Arrows indicate the contributions of polystyrene (blue, ring breathing mode at 1001 cm^{-1}), VA-CNT (black, 2D band of graphenic structure around 2590 cm^{-1}) and LiTFSI (red, CF_3 rocking vibration mode at 275 cm^{-1}). See also Figure S5. (f) Plot of the LiTFSI peak area as a function of the VA-CNT one (both integrated and normalized to the integrated PS peak).

This quantity has then be measured by Quasi-Elastic Neutron Scattering (QENS) [36]. QENS is a powerful experimental technique to probe the dynamics of atoms and molecules at the atomic and molecular scale. The sample is enlighten by a monochromatic neutron beam and as in all scattering technique, a structure factor, $S(Q)$ is measured. Alongside with this structural information, in QENS, the energy of the scattered neutrons is also recorded giving rise to the dynamical structure factor $S(Q,\omega)$ [37].

The neutron scattering process is driven by a nuclear interaction so that strong isotopic effects can be used. Here, the IL moiety is fully hydrogenated. As a consequence, the recorded scattering signal is mainly incoherent and gives insight on the IL cation dynamics at the ps to ns timescale, and in particular on the self-diffusion coefficient, as probed by the individual dynamics of IL protons. As it is closely related to the ionic conductivity by the Nernst-Einstein relation, we are interested in a single quantity: the translational diffusion coefficient of the IL.

3.3.1. QENS: multi-scale dynamics of bulk and CNT confined Omim-Li

In this work, we have used a suite of different neutron spectrometers to probe the electrolyte on a broad dynamical range (from ps to ns).

To analyze the cation dynamics in details, the dynamic structure factor $S(Q,\omega)$ has been measured at 320 K on a extended time scale ranging from 0.1 ps to almost 10 ns (5 orders of magnitude) for both bulk and confined Omim-Li, by combining time-of-flight (ToF), backscattering (BS) and Neutron Spin Echo techniques (NSE).

We have recently shown that IL nanostructuration induces scale dependent transport properties [39]. Due to spontaneous transient self-aggregation process of IL in bulk, the cation dynamics requires a multi-scale analysis to be depicted from the ps to the ms [40]. The model proposed by Ferdeghini et al. describe the alkyl-chain dynamics (rotations and tumbling) and the multi-scale diffusion of the cation: confined diffusion within an aggregate, nanometric diffusion between aggregates and self-diffusion at the micrometer scale. These independent processes are depicted for the bulk IL-Li in Fig. 5. It shows the intermediate scattering function $I(Q,t)$ obtained for bulk Omim-Li obtained following the fitting procedure described in the Supplementary Materials:

$$I(Q,t)^{cation} = I_1(Q)\exp^{(-t/\tau_{SDiff}(Q))} + I_2(Q)\exp^{(-t/\tau_{nano}(Q))}$$
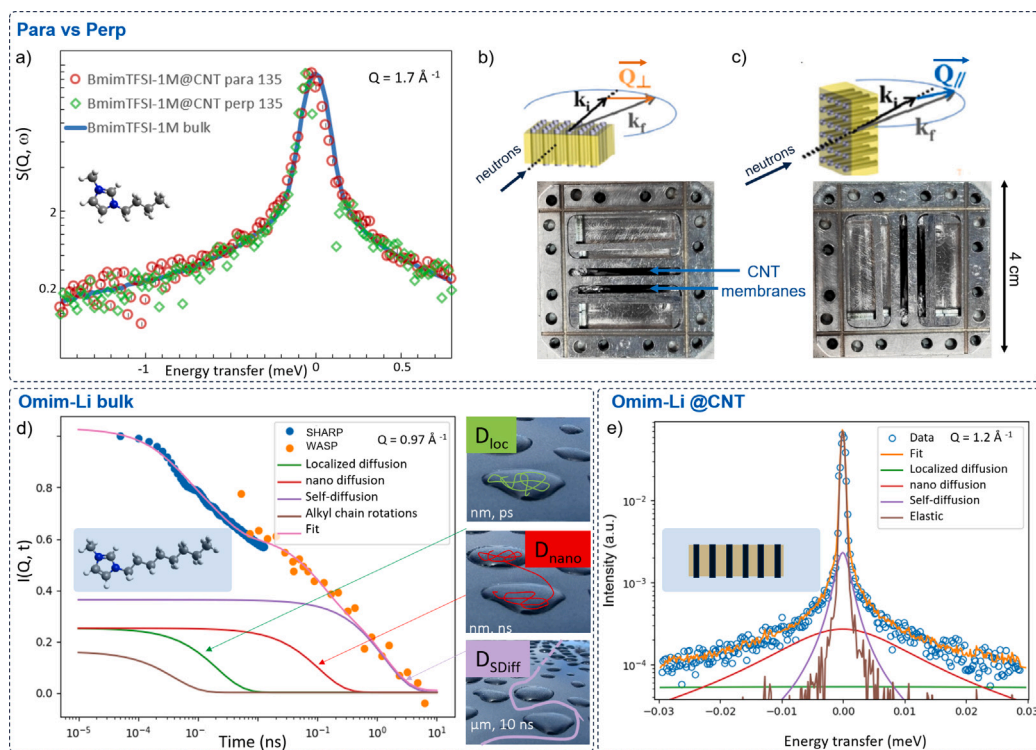$$+ I_3(Q)\exp^{(-t/\tau_{loc}(Q))} + I_4(Q)\exp^{(-t/\tau_{sc}(Q))} \tag{1}$$

Fig. 5. (a) QENS signal (measured on NEAT at HZB) of a bulk IL-Li in bulk, alongside the CNT and perpendicular to the CNT, all showing a similar IL-Li dynamics at the molecular scale (see also Figure S10 and Supplementary Materials for details). Typical experimental aluminum container used to probe the dynamics (b) alongside or (c) perpendicular to the CNT. (d) I(Q = 0.97 Å^{-1}, t) of bulk OmimTFSI 1M LiTFSI fitted with Eq. (1). To be combined with WASP (NSE) data (measured in the time domain) SHARP data (ToF, measured in the energy domain) have been converted to the time domain by Fourier transform. The contribution of the side-chain rotations and tumbling is shown in brown color ($\tau_{sc} = 0.45$ ps ± 0.08 ps), localized diffusion in green ($D_{loc} = 5.0 \pm 0.5 \times 10^{-5}$ cm^2/s), nanometric diffusion ($D_{nano} = 1.0 \pm 0.3 \times 10^{-6}$ cm^2/s) and self-diffusion ($D_{SDiff} = 1.6 \pm 0.3 \times 10^{-7}$ cm^2/s) are shown. The cartoons on the right (adapted from [38]) illustrate the diffusion processes inside or in between the transient IL aggregates. The time and spatial scale probed are indicated. Analysis for extra Q values are shown in Figure S6, S7, S8 and S9. (e) $S(Q,\omega)$ spectra of OmimTFSI 1M LiTFSI under CNT confinement at Q = 0.7 Å^{-1}. The contribution of the alkyl chains rotation and localized diffusion coefficient are unchanged under CNT confinement (Figure S10), but $D_{nano@CNT}$ is found to be 40% higher than in bulk.

where $\tau_i = \hbar/\Gamma_i$, with i = loc, sc and $\tau_j = \hbar(D_j Q^2)^{-1}$ with j = nano, SDiff. The fitting procedure follows the methodology developed by Ferdeghini et al. [40].

The model described accurately the data set from 1 ps to 10 ns (Fig. 5). A precise determination of the nanometric diffusion of the cation in bulk can be inferred:

$D_{nano} = 1.0 \pm 0.3 \times 10^{-6}$ cm^2/s. The localized dynamics of the cation is found to be unchanged compared to its bulk analog (Figure S11). Following a similar strategy to analyze the QENS data of confined Omim-Li (see the Supplementary Materials for details), $D_{nano@CNT}$ is found to be increased by a factor 1.4 (Figure S11). This result seems to show that motions on a scale smaller than the nm are not impacted by the CNT confinement. It is important to note that, in many cases, nanometric confinement results in a slowdown of molecular dynamics, often due to factors such as interactions with the confining matrix and increased tortuosity [41,42].

3.3.2. Confinement effect: activation of the dynamic at lower temperature

Because of the competing contributions from incoherent scattering (primarily from the IL cation) and coherent scattering (mainly from the PS-d matrix), the combination of multi-resolution QENS to study the dynamics of confined IL-Li cannot be applied over the same extended time range as in the case of the bulk material. However, in such a situation, one can use a way-out to assess an accurate value of a diffusion coefficient: a Inelastic Fixed Window Scan (IFWS) strategy. This is a powerful method to get an overview of the dynamical processes at play in a system alongside with their activation energy. The neutrons scattered with a given energy transfer (here 2 μeV, corresponding to dynamical modes with a characteristic time of about 300 ps) are measured upon a slow temperature ramp from 4 to 300 K in 12 h (0.5

K/min). At a given temperature, when a dynamical process activates, the scattered intensity increases until it reaches a maximum. Heating further, the dynamical process becomes too fast to be detectable at the considered energy transfer (here 2 μeV) and the scattered intensity decreases [43].

Fig. 6 shows the data for both bulk and CNT confined Omim-Li and Bmim-Li at Q = 1.26 Å^{-1}. For both electrolytes, in bulk and under confinement, two broad peaks appear (slightly overlapping), centered around approximately 175 K and 280 K. The one at low temperature is non dispersive with Q, i.e. is non Q dependent (the Q dependency of the IFWS is shown in Figure S12–S13). This process is commonly attributed to the activation of the alkyl chain rotation and is not relevant in the present study [44,45].

The peak at higher temperature is dispersive with Q, i.e. Q dependent for both electrolytes, in bulk and under confinement, revealing an underlying diffusive behavior. Interestingly, this dynamical process activates at lower temperature (15–20 K, see ΔT in Table 1 and Fig. 6) under CNT confinement than in bulk. This is a strong evidence of a confinement effect at the nanoscale, consistent with a faster mobility around room temperature under CNT confinement. This finding is crucial for battery applications requiring operation below 0°C.

Next to the qualitative conclusion above, IFWS is also a powerful quantitative method for determination of diffusion coefficients. Following Frick et al. [43,44], the diffusive process can be quantified according to:

$$I^{IFWS} = A \times \frac{\Gamma_1(T)}{\Gamma_1(T)^2 + \omega_{off}^2} + B \times \frac{\Gamma_2(T)}{\Gamma_2(T)^2 + \omega_{off}^2} + C \qquad (2)$$

where Γ_1 and Γ_2 are the HWHM of the two distinct dynamical processes observed in Fig. 6 as broad peaks (centered around 300 K and 175 K,
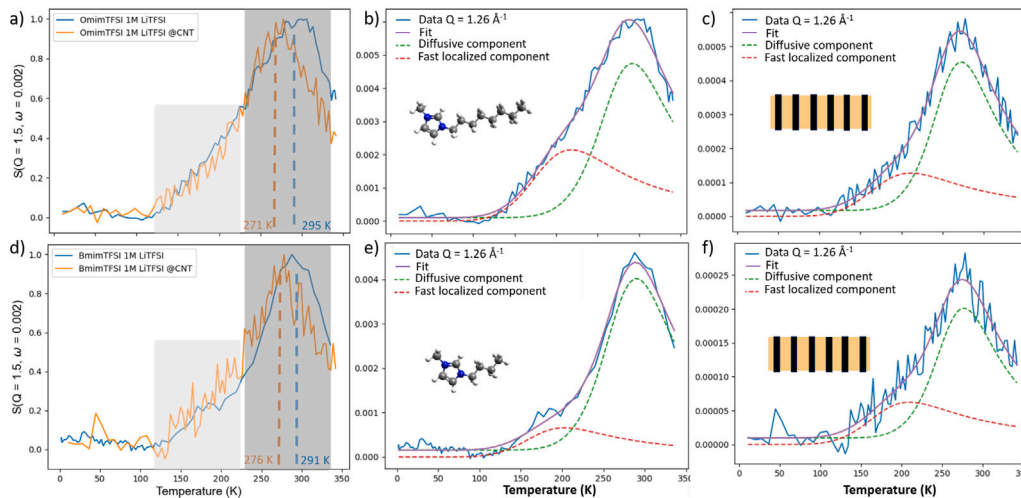
Fig. 6. Inelastic intensities, S(Q = 1.26 Å⁻¹, ω = 2 μeV) of OmimTFSI 1M LiTFSI (top) and BmimTFSI 1M LiTFSI (bottom) in bulk and under CNT confinement. (a) The light and dark gray areas highlight two dynamical processes centered around 175 K and 280 K, respectively (see text). Data are normalized to 1 for comparison. IFWS measured at Q = 1.26 Å⁻¹: bulk and confined Omim-Li (a). Data of bulk (b) and confined (c) Omim-Li are fitted with two Lorentzians (dashed lines). The red Lorentzian corresponds to the rotations of the alkyl chain and methyl groups of the cation. The green Lorentzian corresponds to the diffusive mechanism of the cation. d, e, f: similar plots for bulk and confined Bmim-Li. Fits at 3 Q values for both IL-Li are shown in Figure S12-S13.

Table 1

Diffusion coefficients at 300 K and activation energy obtained fitting the IFWS data with Eq. (2) for both electrolytes, in bulk and under confinement. D_{CNT}/D_{Bulk}, ΔT (temperature difference between the maximum of the IFWS peaks in bulk and under confinement), and E_a are given.

Sample	$D_{300\ K}$ 10^{-7} cm²/s	D_{CNT}/D_{Bulk}	E_a (meV)	ΔT (K)
Omim-Li Bulk	2.5 ± 0.2		183 ± 3	
Omim-Li @CNT	4.4 ± 0.2	1.9 ± 0.3	180 ± 4	20 ± 10
Bmim-Li Bulk	2.5 ± 0.2		190 ± 5	
Bmim-Li @CNT	4.0 ± 0.2	1.6 ± 0.3	185 ± 5	15 ± 7

respectively), A and B scaling factors, ω_{off} the energy transfer of the scattered neutrons (here 2 μeV, C a flat background. We assume that the two dynamical processes follow an Arrhenius behavior. The dispersive signal centered around 300 K accounts for a Fickian diffusion and can be accounted for by $\Gamma_1(T)$ where ($\Gamma_1 = DQ^2$), while the non dispersive follows:

$$D(T) = D_{inf} \times exp\left(\frac{-E_{a_1}}{k.T}\right) \tag{3}$$

$$\Gamma_2(T) = \Gamma_{inf} \times exp\left(\frac{-E_{a_2}}{k.T}\right) \tag{4}$$

where D_{inf} and Γ_{inf} are the high temperature limit of D and Γ_2, respectively.

Fig. 6, shows fitted IFWS data of bulk and CNT confined electrolytes (see Supplementary Materials for details). The fitting parameters are given in Table 1. We have explained above why the QENS analysis measure of the bulk diffusion coefficient is of the order of 10^{-5} and 10^{-6} cm²/s at 320 K while it is in the 10^{-7} cm²/s by NMR. Here, we have chosen only two Lorentzians to describe the multiscale dynamics involving four types of motions according to the QENS analysis. Therefore, the IFWS diffusion coefficients values should not be considered as absolute. They can nevertheless be used as relative values to lead to conclusions on physical behavior on samples measured in the exact same conditions. This is the case in all the samples reported in Table 1. The translational diffusion coefficient at 300 K is higher under confinement by a factor of the order of 2 ± 0.3 for both IL-Li in the time range of few hundreds of ps. It is in good agreement with the QENS results obtained in Section 3.3.1.

3.4. Ionic conductivity

EIS (Electrochemical Impedance Spectroscopy) is commonly used to determine the ionic conductivity of an electrolyte. However, as the CNT are electrical conductors we chose an alternative strategy to measure the conductivity of the confined electrolytes at ambient temperature. The ionic current through the CNT pores has been measured while applying a series of potential (2 to 4 values) across the membrane to determine the overall resistance of the system and the corresponding conductance (Fig. 7). To isolate a smaller number of CNT pores and ensure that the contribution of the confined electrolyte dominates by orders of magnitudes the overall resistance (outweighing contributions from bulk reservoirs and electrodes), a hole was precisely created in the membrane using a Focused Ion Beam (FIB) technique. By refining the parameters of the FIB, holes less than 100 nm up to several microns could be obtained. Prior to the FIB attack, a reduced area (few mm²) was opened using sandpaper in order to maintain mechanical reinforcement around the contour of the membrane, ensuring additional solidity during measurements in the cell. A thin layer of silver of approximately 200 nm was then deposited on this area (Fig. 7a). This layer of silver has a dual role, it allows the upper part of the membrane to be closed and also to ensure good dissipation of charges during the use of the heavy beam, (allowing good focusing of the beam and thus holes of controlled size and small diameter) (see Table 2).

The transport of the electrolyte within these open CNT are the limiting factor of the measured current. The contribution of the bulk electrolytes resistances (in the range of 10^3 Ω for R_{KCl}) are negligible compared to the one attributed to the electrolytes through the CNT (10^6 - 10^8 Ω for $R_{KCl@CNT}$). The sample is inserted between two reservoirs, each equipped with Ag/AgCl electrodes. Electrolyte tightness is ensured by O-rings positioned on either side of the membrane. We apply a DC voltage and we obtain a current response, making it possible to calculate the conductance noted G, which is related to the surface of the open CNT, the length of the CNT, and the electrolyte ionic conductivity (Eq. (5)).

We first measure the conductance of a reference 2.10^{-2} M KCl solution under CNT confinement, $G_{KCl@CNT}$, which we consider not impacted by nanometric confinement. This value can be considered as a normalization factor standing for the active surface area of opened
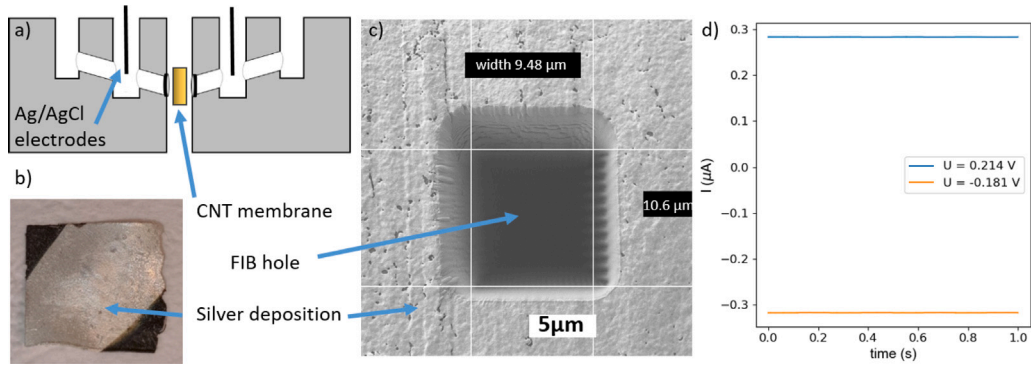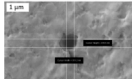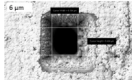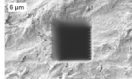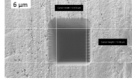
Fig. 7. (a) Cut view of the electrochemical set-up. The CNT membrane is pressed between two o-rings, with reservoirs containing the electrolyte and Ag/AgCl electrodes on each side. (b) Picture of the 1 cm^2 CNT membrane with silver deposition. (c) SEM image of hole made by FIB on the silver. d) Current measured as a function of time: $G_{Omim-Li~@CNT} = 1.52 \times 10^{-6}$ S. In the same conditions $G_{KCl@CNT} = 1.43 \times 10^{-6}$ S leading to $\sigma_{Omim-Li@CNT} = 2.9 \times 10^{-3}$ S cm^{-1} and Gain = 7.9.

Table 2

SEM images of the CNT membrane open by FIB, open surface area. Conductance (G) under confinement of KCl and Omim-Li. Omim-Li conductivity under confinement and conductivity gain (when compared to $\sigma_{Omim-Li~bulk} = 3.66 \times 10^{-4}$ S/cm).

SEM image	Open surface (cm^2)	G_{KCl} (S)	$G_{Omim-Li}$ (S)	$\sigma_{Omim-Li}$ (mS cm^{-1})	Gain
	9.62×10^{-10}	3.47×10^{-9}	1.43×10^{-8}	11.1	30.4
	3.71×10^{-7}	5.21×10^{-8}	1.67×10^{-7}	8.66	23.7
	8.10×10^{-7}	1.32×10^{-8}	1.47×10^{-8}	3.00	8.19
	9.00×10^{-7}	1.43×10^{-6}	1.52×10^{-6}	2.87	7.84
	1.00×10^{-6}	1.37×10^{-6}	1.68×10^{-6}	3.30	9.02

CNT, S_{CNT}, and their length, $L_{CNT} = 100$ μm. This value is therefore used as a reference to determine S_{CNT} (given in Table C.2):

$$S_{CNT} = \frac{G_{KCl@CNT} \times L_{CNT}}{\sigma_{KCl~bulk}} \qquad (5)$$

The same membrane is then thoroughly cleaned with distilled water, dried under a secondary vacuum, and subsequently immersed in the Omim-Li electrolyte. The ratio L_{CNT}/S_{CNT} beeing constant for KCl and Omim-Li, the conductivity of the confined electrolytes writes:

$$\sigma_{Omim-Li@CNT} = \frac{\sigma_{KCl~bulk} \times G_{Omim-Li@CNT}}{G_{KCl@CNT}} \qquad (6)$$

where $\sigma_{KCl~bulk} = (2.7 \pm 0.1).10^{-3}$ S cm^{-1}.

The conductivity gain is defined as the ratio of confined and bulk conductivity:

$$Gain = \sigma_{Omim-Li@CNT}/\sigma_{Omim-Li~bulk} \qquad (7)$$

where $\sigma_{Omim-Li~bulk} = (3.7 \pm 0.1) \times 10^{-4}$ S cm^{-1} (measured with a Jenway™ conductivity cell). On average, at room temperature, on 5 different membranes with large variation of opened CNT areas, we find a conductivity gain of 16 ± 9 (see Table 2 for hole size, conductance, conductivity and gain for each measurements). This remarkable outcome aligns with the trend observed at the molecular scale, where charge transport properties are enhanced under CNT confinement. On the macroscopic level, this effect is dramatic, resulting in a tenfold increase in conductivity. To get insights in the underlying physical mechanisms, we conducted Molecular Dynamics (MD) simulations.

3.5. Molecular dynamics

All the techniques used so far in this study only provide a partial probe of the different dynamical processes and an average view of the physical processes at work in the system. MD can offer an intimate view of these phenomena, in particular of all the individual components.

These molecular dynamics simulations are used to extract the radial density inside the 4 nm diameter CNT tube (Fig. 8), which is longer than the size of the molecules and the nanostructure (Bmim ~ 0.8 nm, Omim ~ 1.3 nm, TFSI ~ 0.6 nm, nanosegregation ~ 1.8 nm) [10,46]. This representation highlights a particular distribution of the different moieties of the Bmim-Li. The latter are organized in a concentric zone on the internal wall of the CNT. This core shell cylindrical organization delineates preferential zones for ions and in particular lithium diffusion. Despite a modified nanostructure, the radial distribution functions show that the local environment of ions is almost not altered by the confinement (Fig. 8c). This is perfectly in line with QENS that showed no modification of the fast localized dynamics at the molecular level Figure S10.

As discussed in Section 1, the ratio Φ_{Pore}/a (here ~ 2) is a crucial parameter when addressing nanoconfinement. Reducing this ratio can be achieved either by increasing the alkyl chain length or by decreasing the pore diameter. For Omim-Li, which exhibits a more pronounced bulk nanostructure due to its longer alkyl chain, we can expect a similar or even more pronounced distribution of components compared to Bmim-Li. Furthermore, when decreasing the CNT diameter, Pensado et al. have demonstrated a more defined core–shell structure in Bmim base IL [47]. In both scenarios, the disruption of IL-Li's natural self-organization could potentially create well-defined channels that further
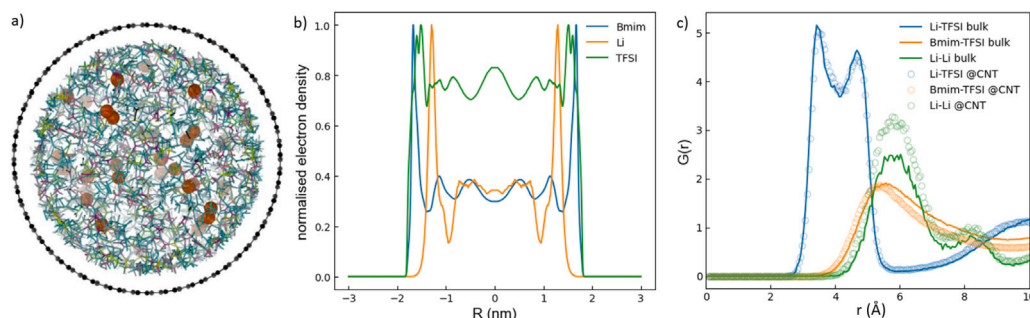
Fig. 8. (a) Cross section of a CNT filled with BmimTFSI 1M LiTFSI and (b) corresponding radial distribution (normalized to 1) of the electronic density of Bmim, TFSI and Li. (c) Comparison of the radial distribution function G(r) of Bmim-Li in bulk and under CNT confinement.

enhance lithium diffusion. This hypothesis might explain the tenfold increase in ionic conductivity observed in the previous section.

4. Perspectives

The CNT membrane we have developed so far could be optimized, and we have identified several key possible improvements. After synthesis, the CNT forests exhibit a relatively low surface density (around 5%). However, using a densification process described in the literature [48], it is possible to increase the surface density of the CNT forests to 80%. This is a crucial step for maximizing the amount of confined electrolyte. Additionally, minimizing the reorganization of the neat VA-CNT that occurs during the pouring of the PS matrix onto the CNT network would be advantageous (Fig. 4a). To address this, we have proposed an additive synthesis step to maintain the CNT tips before pouring [49,50].

A critical requirement for using CNT membranes as battery separators is to prevent any short-circuits. This could be accomplished through chemical grafting of the CNT, which would modify their sp^2 hybridization. In the case of multi-walled (MW) CNT, such chemical modifications would only affect the outer CNT layer, while the inner CNT within the MW assembly would retain their electronic conductivity. To address this issue, in the current project, poly-IL chains have been grafted onto the CNT caps using the *grafted from* method. This approach ensures both efficient ionic conduction at the CNT pore entrances and electrical insulation at the CNT/electrode interface. We have verified that this nanometric layer effectively prevents electrical shorts between the electrodes [51]. This work, which extends beyond the scope of this paper, will be published elsewhere. Additionally, a patent has been filed on the solid-state battery separator membrane presented in this study [49,52].

While the observed one-order-of-magnitude improvement in ionic transport properties offers a clear advantage for enhancing specific power, it is important to note that this gain could be compromised at the electrodes. A promising strategy to further boost the performance of lithium metal batteries involves the use of VA-CNT-based 1D electrodes [53]. Combining these 1D electrodes with the 1D separator could enable the creation of an entirely 1D lithium metal battery system, potentially addressing the current gap in the Ragone plot by delivering both high power and high energy density in batteries.

5. Conclusion

We have developed a polymeric nanoporous composite membrane based on VA-CNT forests. The porosity of this system originates from a network of parallel CNT oriented perpendicularly to the membrane surface, creating 1D diffusion pathways for ions. Through PFG-NMR, neutron imaging, SEM-EDX, and Raman scattering analyses, we have demonstrated that the imidazolium based IL (BmimTFSI and OmimTFSI) charged with 1M LiTFSI do not infiltrate the PS component of the membrane. Instead, these IL-Li are confined solely within the 1D porous

network formed by the interior of the CNT. It has been further confirmed by observing an activation of the dynamics at lower temperature under confinement through neutron IFWS.

We conducted an innovative conductivity characterization using a patch-clamp inspired method. Our findings reveal a significant enhancement in the ionic conductivity of Omim-Li when confined within 1D CNT membranes, demonstrating an order of magnitude increase compared to the bulk situation. To understand the underlying mechanism of this phenomenon, we performed a multi-scale study of the IL-Li dynamics in both bulk and confined state, combining PFG-NMR (μm / ms) and neutron scattering techniques (QENS, NSE: ps - ns / Å- nm). At the molecular level, we observed a twofold increase in the nanometric translational diffusion coefficient of the cation, along with a shift in the activation of IL-Li dynamics, occurring 10 to 20 K lower than in the bulk. This observation holds great potential for enabling high-performance batteries that can operate efficiently at lower temperatures.

Molecular dynamics results strongly indicate that the observed conductivity gain could be attributed to a significant reorganization of the electrolyte under confinement. The electrolyte is organized along the axis of the CNT and forms concentric cylindrical domains. The low density zones could creates preferential pathways facilitating enhanced lithium-ion conductivity. Although the VA-CNT membranes presented in this work demonstrate significantly improved conductivity, their high production costs could represent a barrier to their commercial viability for consumer applications. Our primary objective here is to emphasize the concept of 1D nanometric confinement combined with macroscopic orientation. We propose that nanoporous composite membrane composed of macroscopic 1D diffusion channels loaded with non-flammable electrolytes represent a promising separator for next generation "all-solid-state" batteries.

CRediT authorship contribution statement

Nino Modesto: Writing – original draft, Visualization, Methodology, Investigation, Formal analysis. **Camille Pinchart:** Writing – original draft, Validation, Methodology, Investigation, Formal analysis. **Mohammad Abdel Sater:** Writing – original draft, Investigation, Formal analysis. **Markus Appel:** Writing – original draft, Methodology, Formal analysis. **Peter Fouquet:** Writing – original draft, Methodology, Formal analysis. **Alessandro Tengattini:** Writing – original draft, Methodology, Formal analysis. **Margarita Russina:** Writing – original draft, Resources, Formal analysis. **Veronika Grzimek:** Writing – original draft, Resources. **Gerrit Günther:** Writing – original draft, Visualization, Resources. **Pierre-Henri Jouneau:** Writing – original draft, Visualization, Supervision, Investigation. **Benoit Coasne:** Writing – original draft, Visualization, Resources, Methodology, Formal analysis. **Didier Lairez:** Writing – original draft, Software, Resources, Methodology, Formal analysis. **Patrick Judeinstein:** Writing – original draft, Supervision, Resources, Investigation, Formal analysis. **Raphael Ramos:** Writing – review & editing, Writing – original draft, Validation,

Supervision, Resources, Methodology, Investigation, Formal analysis. **Didier Gigmes:** Writing – original draft, Supervision, Resources, Funding acquisition. **Trang N.T. Phan:** Writing – original draft, Supervision, Methodology. **Quentin Berrod:** Writing – review & editing, Writing – original draft, Visualization, Validation, Supervision, Resources, Project administration, Methodology, Investigation, Funding acquisition, Formal analysis, Data curation, Conceptualization. **Jean-Marc Zanotti:** Writing – review & editing, Writing – original draft, Validation, Supervision, Software, Resources, Project administration, Investigation, Funding acquisition, Formal analysis, Conceptualization.

Declaration of competing interest

The authors declare that they have no known competing financial interests or personal relationships that could have appeared to influence the work reported in this paper.

Acknowledgments

Appendix A. Supplementary data

Supplementary material related to this article can be found online at https://doi.org/10.1016/j.ensm.2025.104045.

Data availability

Data will be made available on request.

References

[1] S.Y. Lai, C. Cavallo, M.E. Abdelhamid, F. Lou, A.Y. Koposov, Advanced and emerging negative electrodes for Li-ion capacitors: pragmatism vs. performance, Energies 14 (11) (2021) 3010.

[2] Z. Zhang, W.-Q. Han, From liquid to solid-state lithium metal batteries: Fundamental issues and recent developments, Nano-Micro Lett. 16 (1) (2023) 24, http://dx.doi.org/10.1007/s40820-023-01234-y.

[3] Safer Electrolytes for Lithium-Ion Batteries: State of the Art and Perspectives, vol. 8.

[4] J. Janek, W.G. Zeier, Challenges in speeding up solid-state battery development, Nat. Energy 8 (3) (2023) 230–240, http://dx.doi.org/10.1038/s41560-023-01208-9, Number: 3 Publisher: Nature Publishing Group, URL https://www.nature.com/articles/s41560-023-01208-9.

[5] Y. Feng, L. Zhou, H. Ma, Z. Wu, Q. Zhao, H. Li, K. Zhang, J. Chen, Challenges and advances in wide-temperature rechargeable lithium batteries, Energy Environ. Sci. 15 (5) (2022) 1711–1759, http://dx.doi.org/10.1039/D1EE03292E, Publisher: The Royal Society of Chemistry, URL https://pubs.rsc.org/en/content/articlelanding/2022/ee/d1ee03292e.

[6] T. Jin, G. Singer, K. Liang, Y. Yang, Structural batteries: Advances, challenges and perspectives, Mater. Today 62 (2023) 151–167, http://dx.doi.org/10.1016/j.mattod.2022.12.001, URL https://www.sciencedirect.com/science/article/pii/S1369702122003364.

[7] M. Dong, K. Zhang, X. Wan, S. Wang, S. Fan, Z. Ye, Y. Wang, Y. Yan, X. Peng, Stable two-dimensional nanoconfined ionic liquids with highly efficient ionic conductivity, Small 18 (14) (2022) 2108026, http://dx.doi.org/10.1002/smll.202108026, _eprint: https://onlinelibrary.wiley.com/doi/pdf/10.1002/smll.202108026, URL https://onlinelibrary.wiley.com/doi/abs/10.1002/smll.202108026.

[8] A. Triolo, O. Russina, H.-J. Bleif, E. Di Cola, Nanoscale segregation in room temperature ionic liquids †, J. Phys. Chem. B 111 (18) (2007) 4641–4644, http://dx.doi.org/10.1021/jp067705t.

[9] P. Judeinstein, M. Zeghal, D. Constantin, C. Iojoiu, B. Coasne, Interplay of structure and dynamics in lithium/ionic liquid electrolytes: Experiment and molecular simulation, J. Phys. Chem. B 125 (6) (2021) 1618–1631, http://dx.doi.org/10.1021/acs.jpcb.0c09597, Publisher: American Chemical Society, URL https://hal.science/hal-03201489.

[10] A. Martinelli, M. Maréchal, A. Ostlund, J. Cambedouzou, Insights into the interplay between molecular structure and diffusional motion in 1-alkyl-3-methylimidazolium ionic liquids: a combined PFG NMR and X-ray scattering study, Phys. Chem. Chem. Phys. 15 (15) (2013) 5510–5517, http://dx.doi.org/10.1039/C3CP00097D.

[11] F. Ferdeghini, Q. Berrod, J.-M. Zanotti, P. Judeinstein, V. García Sakai, O. Czakkel, P. Fouquet, D. Constantin, Nanostructuration of ionic liquids: impact on the cation mobility. A multi-scale study, Nanoscale 9 (5) (2017) 1901–1908, http://dx.doi.org/10.1039/C6NR07604A, Publisher: Royal Society of Chemistry, URL https://pubs.rsc.org/en/content/articlelanding/2017/nr/c6nr07604a.

[12] A.I. Kolesnikov, J.-M. Zanotti, C.-K. Loong, P. Thiyagarajan, A.P. Moravsky, R.O. Loutfy, C.J. Burnham, Anomalously soft dynamics of water in a nanotube: A revelation of nanoscale confinement, Phys. Rev. Lett. 93 (3) (2004) 035503, http://dx.doi.org/10.1103/PhysRevLett.93.035503, URL https://link.aps.org/doi/10.1103/PhysRevLett.93.035503.

[13] J.K. Holt, H.G. Park, Y. Wang, M. Stadermann, A.B. Artyukhin, C.P. Grigoropoulos, A. Noy, O. Bakajin, Fast mass transport through Sub-2-nanometer carbon nanotubes, Science 312 (5776) (2006) 1034–1037, http://dx.doi.org/10.1126/science.1126298.

[14] K. Falk, F. Sedlmeier, L. Joly, R.R. Netz, L. Bocquet, Molecular origin of fast water transport in carbon nanotube membranes: Superlubricity versus curvature dependent friction, Nano Lett. 10 (10) (2010) 4067–4073, http://dx.doi.org/10.1021/nl1021046, Publisher: American Chemical Society.

[15] W. Nernst, Die elektrolytischen Lösungen, Z. Phys. Chem. 4 (1889) 129–181.

[16] A. Einstein, Über die von der molekularkinetischen Theorie der Wärme geforderte Bewegung von in ruhenden Flüssigkeiten suspendierten Teilchen, Ann. Phys. 322 (8) (1905) 549–560.

[17] P. Atkins, J.D. Paula, J. Keeler, Atkins' Physical Chemistry, twenth ed., Oxford University Press, 2022, http://dx.doi.org/10.1093/hesc/9780198847816.001.0001, URL https://www.oxfordsciencetrove.com/view/10.1093/hesc/9780198847816.001.0001/isbn-9780198847816.

[18] Q. Berrod, F. Ferdeghini, P. Judeinstein, N. Genevaz, R. Ramos, A. Fournier, J. Dijon, J. Ollivier, S. Rols, D. Yu, R.A. Mole, J.-M. Zanotti, Enhanced ionic liquid mobility induced by confinement in 1D CNT membranes, Nanoscale 8 (15) (2016) 7845–7848, http://dx.doi.org/10.1039/C6NR01445C, Publisher: The Royal Society of Chemistry, URL https://pubs.rsc.org/en/content/articlelanding/2016/nr/c6nr01445c.

[19] F. Ferdeghini, Liquides Ioniques Sous Confinement Nanométrique Unidimensionnel (Ph.D. thesis), Université Paris Saclay, 2015.

[20] J. Dijon, P.D. Szkutnik, A. Fournier, T. Goislard de Monsabert, H. Okuno, E. Quesnel, V. Muffato, E. De Vito, N. Bendiab, A. Bogner, N. Bernier, How to switch from a tip to base growth mechanism in carbon nanotube growth by catalytic chemical vapour deposition, Carbon 48 (13) (2010) 3953–3963, http://dx.doi.org/10.1016/j.carbon.2010.06.064, URL https://www.sciencedirect.com/science/article/pii/S0008622310004707.

[21] J.-M. Zanotti, Q. Berrod, P. Judeinstein, Ionic liquid under 1D nanometric confinement in CNT membranes: gigantic transport properties? Inst. Laue-Langevin (ILL) (2018) http://dx.doi.org/10.5291/ILL-DATA.CRG-2483.

[22] J.-M. Zanotti, C. Pinchart, N. Modesto, P. Judeinstein, Q. Berrod, Dynamics of a polymer electrolyte in bulk and under 1D CNT nanometricconfinement, Inst. Laue-Langevin (ILL) (2018) http://dx.doi.org/10.5291/ILL-DATA.CRG-2908.

[23] Q. Berrod, M. Abdelsater, M. Appel, D. Gigmes, P. Judeinstein, N. Modesto, J. Ollivier, T.N.T. Phan, C. Pinchart, R. Ramos, J.-M. Zanotti, Enhanced ionic liquid mobility induced by confinement in 1D carbone NanoTube membranes, Inst. Laue-Langevin (ILL) (2021) http://dx.doi.org/10.5291/ILL-DATA.6-07-84.

[24] J.-M. Zanotti, Q. Berrod, J. Dijon, F. Ferdeghini, F. Fouquet, P. Judeinstein, Ionic liquids under 1D nanometric confinement in CNT membranes: gigantic transport properties? Inst. Laue-Langevin (ILL) (2018) http://dx.doi.org/10.5291/ILL-DATA.6-07-30.

[25] C. Pinchart, M. Abdelsater, Q. Berrod, P. Fouquet, D. Gigmes, P. Judeinstein, N. Modesto, T.N.T. Phand, R. Ramos, F. Saint-Antonin, J.-M. Zanotti, Dynamics of a polymer electrolyte in bulk and under 1D CNT nanometric confinement, Inst. Laue-Langevin (ILL) (2021) http://dx.doi.org/10.5291/ILL-DATA.6-07-64.

[26] M. Russina, G. Guenther, V. Grzimek, R. Gainov, M.-C. Schlegel, L. Drescher, T. Kaulich, W. Graf, B. Urban, A. Daske, et al., Upgrade project NEAT 2016 at Helmholtz Zentrum Berlin. What can be done on the medium power neutron source, Phys. B 551 (2018) 506–511.

[27] G. Günther, M. Russina, Background optimization for the neutron time-of-flight spectrometer NEAT, Nucl. Instrum. Methods Phys. Res. A 828 (2016) 250–261.

[28] O. Arnold, J. Bilheux, J. Borreguero, A. Buts, S. Campbell, L. Chapon, M. Doucet, N. Draper, R.F. Leal, M. Gigg, V. Lynch, A. Markvardsen, D. Mikkelson, R. Mikkelson, R. Miller, K. Palmen, P. Parker, G. Passos, T. Perring, P. Peterson, S. Ren, M. Reuter, A. Savici, J. Taylor, R. Taylor, R. Tolchenov, W. Zhou, J. Zikovsky, Mantid—Data analysis and visualization package for neutron scattering and muSR experiments, Nucl. Instrum. Methods Phys. Res. A 764 (2014) 156–166, http://dx.doi.org/10.1016/j.nima.2014.07.029, URL http://www.sciencedirect.com/science/article/pii/S0168900214008729.

[29] Igor Pro 9 software (WaveMetrics, Portland).

[30] J.N. Canongia Lopes, J. Deschamps, A.A.H. Pádua, Modeling ionic liquids using a systematic all-atom force field, J. Phys. Chem. B 108 (30) (2004) 11250, http://dx.doi.org/10.1021/jp0476996, Publisher: American Chemical Society.

[31] X. Wu, Z. Liu, S. Huang, W. Wang, Molecular dynamics simulation of room-temperature ionic liquid mixture of [bmim][BF 4] and acetonitrile by a refined force field, Phys. Chem. Chem. Phys. 7 (14) (2005) 2771–2779.

[32] C. Merlet, B. Rotenberg, P.A. Madden, P.-L. Taberna, P. Simon, Y. Gogotsi, M. Salanne, On the molecular origin of supercapacitance in nanoporous carbon electrodes, Nature Mater. 11 (4) (2012) 306–310.

[33] P. Judeinstein, M. Zeghal, D. Constantin, C. Iojoiu, B. Coasne, Interplay of structure and dynamics in Lithium/Ionic liquid electrolytes: Experiment and molecular simulation, J. Phys. Chem. B 125 (6) (2021) 1618–1631.

[34] F. Lange, P. Judeinstein, C. Franz, B. Hartmann-Azanza, S. Ok, M. Steinhart, K. Saalwächter, Large-scale diffusion of entangled polymers along nanochannels, ACS Macro Lett. 4 (5) (2015) 561–565.

[35] H. Wang, D. Ning, L. Wang, H. Li, Q. Li, M. Ge, J. Zou, S. Chen, H. Shao, Y. Lai, Y. Zhang, G. Xing, W.K. Pang, Y. Tang, In operando neutron scattering multiple-scale studies of lithium-ion batteries, Small 18 (19) (2022) 2107491, http://dx.doi.org/10.1002/smll.202107491, _eprint: https://onlinelibrary.wiley.com/doi/pdf/10.1002/smll.202107491, URL https://onlinelibrary.wiley.com/doi/abs/10.1002/smll.202107491.

[36] M. Bée, Quasielastic Neutron Scattering, Adam Hilger, 1988.

[37] Q. Berrod, K. Lagrené, J. Ollivier, J.-M. Zanotti, Inelastic and quasi-elastic neutron scattering. Application to soft-matter, in: M. Wolff, F. Cousin (Eds.), EPJ Web Conf. 188 (2018) 05001, http://dx.doi.org/10.1051/epjconf/201818805001, URL https://www.epj-conferences.org/10.1051/epjconf/201818805001.

[38] Q. Berrod, F. Ferdeghini, J.-M. Zanotti, P. Judeinstein, D. Lairez, V. García Sakai, O. Czakkel, P. Fouquet, D. Constantin, Ionic Liquids: evidence of the viscosity scale-dependence, Sci. Rep. 7 (2017) http://dx.doi.org/10.1038/s41598-017-02396-7, URL http://www.ncbi.nlm.nih.gov/pmc/articles/PMC5440414/.

[39] Q. Berrod, F. Ferdeghini, J.-M. Zanotti, P. Judeinstein, D. Lairez, S.V. García, O. Czakkel, P. Fouquet, D. Constantin, Ionic liquids: evidence of the viscosity scale-dependence, Sci. Rep. 7 (1) (2017) 2241.

[40] F. Ferdeghini, Q. Berrod, J.-M. Zanotti, P. Judeinstein, V.G. Sakai, O. Czakkel, P. Fouquet, D. Constantin, Nanostructuration of ionic liquids: impact on the cation mobility. A multi-scale study, Nanoscale 9 (5) (2017) 1901–1908.

[41] L.J. Michot, A. Delville, B. Humbert, M. Plazanet, P. Levitz, Diffusion of water in a synthetic clay with tetrahedral charges by combined neutron time-of-flight measurements and molecular dynamics simulations, J. Phys. Chem. C 111 (27) (2007) 9818–9831.

[42] J.-C. Perrin, S. Lyonnard, F. Volino, A. Guillermo, Gaussian model for localized translational motion. Application to water dynamics in Nafion® studied by quasi-elastic neutron scattering, Eur. Phys. J. Spec. Top. 141 (1) (2007) 57–60, http://dx.doi.org/10.1140/epjst/e2007-00017-y, URL http://link.springer.com/article/10.1140/epjst/e2007-00017-y.

[43] B. Frick, J. Combet, L. Van Eijck, New possibilities with inelastic fixed window scans and linear motor Doppler drives on high resolution neutron backscattering spectrometers, Nucl. Instrum. Methods Phys. Res. A 669 (2012) 7–13.

[44] M. Busch, T. Hofmann, B. Frick, J.P. Embs, B. Dyatkin, P. Huber, Ionic liquid dynamics in nanoporous carbon: A pore-size-and temperature-dependent neutron spectroscopy study on supercapacitor materials, Phys. Rev. Mater. 4 (5) (2020) 055401.

[45] T. Burankova, E. Reichert, V. Fossog, R. Hempelmann, J.P. Embs, The dynamics of cations in pyridinium-based ionic liquids by means of quasielastic-and inelastic neutron scattering, J. Mol. Liq. 192 (2014) 199–207.

[46] L. Aguilera, J. Völkner, A. Labrador, A. Matic, The effect of lithium salt doping on the nanostructure of ionic liquids, Phys. Chem. Chem. Phys. 17 (40) (2015) 27082–27087, http://dx.doi.org/10.1039/C5CP03825A.

[47] A.S. Pensado, F. Malberg, M.C. Gomes, A.A. Pádua, J. Fernández, B. Kirchner, Interactions and structure of ionic liquids on graphene and carbon nanotubes surfaces, RSC Adv. 4 (35) (2014) 18017–18024.

[48] B. Lee, Y. Baek, M. Lee, D.H. Jeong, H.H. Lee, J. Yoon, Y.H. Kim, A carbon nanotube wall membrane for water treatment, Nat. Commun. 6 (1) (2015) 7109, http://dx.doi.org/10.1038/ncomms8109, URL https://www.nature.com/articles/ncomms8109.

[49] A. Bélime, Q. Berrod, R. Ramos, J.-M. Zanotti, CNT Based Porous Composite Membrane for Electrolyte Confinement (03/2020): Procédé de fabrication d'une membrane à électrolytes, (no. FR2002224) 2020.

[50] S. Kim, F. Fornasiero, H.G. Park, J.B. In, E. Meshot, G. Giraldo, M. Stadermann, M. Fireman, J. Shan, C.P. Grigoropoulos, et al., Fabrication of flexible, aligned carbon nanotube/polymer composite membranes by in-situ polymerization, J. Membr. Sci. 460 (2014) 91–98.

[51] N. Modesto, Smart Membranes Pour Batteries Lithium-Métal-Polymère (Ph.D. thesis), Université Grenoble Alpes, 2022, URL https://www.theses.fr/2022GRALY087.

[52] J.-M. Zanotti, Q. Berrod, J. Dijon, F. Ferdeghini, P. Judeinstein, Membrane poreuse à électrolyte, son procédé de préparation, et dispositifs électrochimiques la comprenant, (no. WO2016151142A1) 2016, URL https://patents.google.com/patent/WO2016151142A1/fr?oq=WO2016151142.

[53] Y. Cai, Y. Wang, L. Cheng, S. Guo, T. Liu, Z. Hu, H. Yu, D. Chen, Y. Li, H. Yuan, Structure design and assembly mode of carbon nanotube-based flexible electrode materials and flexible supercapacitors, J. Energy Storage 73 (2023) 109179, http://dx.doi.org/10.1016/j.est.2023.109179, URL https://linkinghub.elsevier.com/retrieve/pii/S2352152X2302577X.